


SCIENTIFIC REPORTS



OPEN

Mirror-symmetry protected non-TRIM surface state in the weak topological insulator Bi_2TeI

I. P. Rusinov^{1,2}, T. V. Menshchikova¹, A. Isaeva³, S. V. Ereemeev^{1,2,4}, Yu. M. Koroteev^{1,4}, M. G. Vergniory⁵, P. M. Echenique^{5,6,7} & E. V. Chulkov^{1,2,5,6,7}

Received: 17 November 2015

Accepted: 06 January 2016

Published: 11 February 2016

Strong topological insulators (TIs) support topological surface states on any crystal surface. In contrast, a weak, time-reversal-symmetry-driven TI with at least one non-zero $\nu_1, \nu_2, \nu_3 \mathbb{Z}_2$ index should host spin-locked topological surface states on the surfaces that are not parallel to the crystal plane with Miller indices $(\nu_1 \nu_2 \nu_3)$. On the other hand, mirror symmetry can protect an even number of topological states on the surfaces that are perpendicular to a mirror plane. Various symmetries in a bulk material with a band inversion can independently preordain distinct crystal planes for realization of topological states. Here we demonstrate the first instance of coexistence of both phenomena in the weak 3D TI Bi_2TeI which $(\nu_1 \nu_2 \nu_3)$ surface hosts a gapless spin-split surface state protected by the crystal mirror-symmetry. The observed topological state has an even number of crossing points in the $\bar{\Gamma} - \bar{M}$ directions of the 2D Brillouin zone due to a non-TRIM bulk-band inversion. Our findings shed light on hitherto uncharted features of the electronic structure of weak topological insulators and open up new vistas for applications of these materials in spintronics.

The gapless spin-polarized states of topological insulators (TIs) at the edge (in two-dimensional (2D) TIs) or at the surface (in three-dimensional (3D) TIs) open up exciting possibilities for applications of these materials in spintronics^{1–3}. The \mathbb{Z}_2 classification of TIs is based on topological invariants $(\nu_0; \nu_1 \nu_2 \nu_3)$ and allows to attribute 3D TIs to one of two classes. The $\nu_0 = 1$ identifies strong TIs, which are characterized by metallic surface states forming an odd number of Dirac cones. These states are robust against perturbations that do not break the time-reversal symmetry. The non-zero ν_1, ν_2 and ν_3 indices define (at $\nu_0 = 0$) so-called weak TIs that have an even number of Dirac cones. Spin-locked topological surface states (TSSs) in weak TIs should exist on any crystal surface which is not parallel to the plane with Miller indices $(\nu_1 \nu_2 \nu_3)$ ⁴. The surface states of a weak TI exhibit weaker topological protection than those of a strong TI and can be gapped without breaking the time-reversal symmetry⁵.

In contrast to the extensive studies on strong 3D TIs, only a limited number of accounts on electronic properties of weak TIs is available at present, e.g. honeycomb compounds XYZ ($X = \text{K, Na, Li}$; $Y = \text{Hg, Cd/Au, Ag}$; $Z = \text{Sb, As, P/Te, Se}$)⁶, a theoretically modelled octahedron-decorated cubic lattice⁷, PbTe/SnTe superlattices⁸, $\text{Bi}_{14}\text{Rh}_3\text{I}_9$ ^{9–11}, and Bi_2TeI ¹². With an exception of refs 9, 11, the above-mentioned papers do not address the $(\nu_1 \nu_2 \nu_3)$ crystal surface.

Classes of materials with non-trivial band structures are not restricted to \mathbb{Z}_2 TIs. So-called topological crystal-line insulators (TCI) represent another type of topological insulating materials with a band gap inverted by the strong spin-orbit coupling (SOC). However, the topological phase therein is protected by a symmetry differing from the time-reversal symmetry, namely by the crystal mirror symmetry^{13,14}. Consequently, these materials possess topologically protected surface states on the surfaces that are perpendicular to the mirror plane.

¹Tomsk State University, pr. Lenina, 36, Tomsk, 634050 Russia. ²St. Petersburg State University, Universitetskaya nab., 7/9, St. Petersburg, 199034 Russia. ³Technische Universität Dresden, Bergstraße, 66, Dresden, D-01069, Germany. ⁴Institute of Strength Physics and Materials Science, pr. Akademicheskiiy, 2/4, Tomsk, 634021 Russia. ⁵Donostia International Physics Center (DIPC), Paseo de Manuel Lardizabal, 4, 20018 San Sebastián/Donostia, Basque Country, Spain. ⁶Departamento de Física de Materiales, Facultad de Ciencias Químicas, UPV/EHU, 20080 San Sebastián/Donostia, Basque Country, Spain. ⁷Centro de Física de Materiales CFM-MPC, Centro Mixto CSIC-UPV/EHU, 20080 San Sebastián/Donostia, Basque Country, Spain. Correspondence and requests for materials should be addressed to I.P.R. (email: rusinovip@gmail.com)

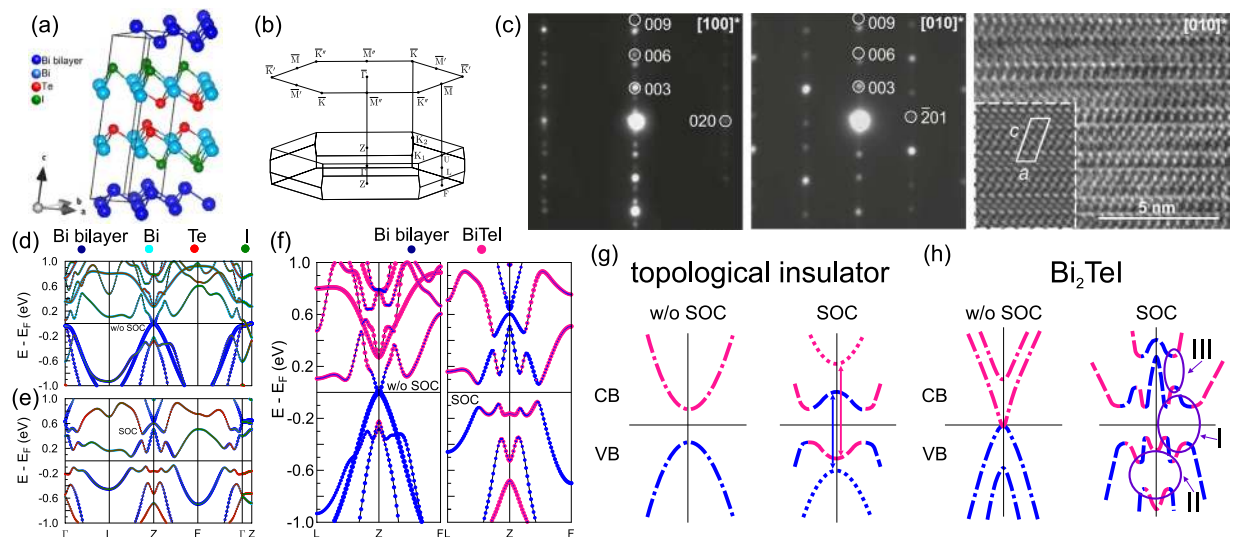


Figure 1. Crystal structure and bulk electronic spectrum of the Bi_2Te_1 . (a) A view of the Bi_2Te_1 crystal structure. (b) The 3D and 2D Brillouin zones of a Niggli-reduced cell. (c) Experimental diffraction patterns of the $[100]^*$ (left) and the $[010]^*$ (centre) zones for a 50 nm thick lamella cut out from a Bi_2Te_1 crystal. Right: a HRTEM image of the $[010]^*$ zone with an inserted simulated HRTEM ($d = 28$ nm, $t = 10$ nm) outlined by a white dashed line. According to simulations, the bright spots correspond to atoms. The unit cell is outlined by a solid white line. Bulk band spectra of Bi_2Te_1 calculated without (d) and with (e) SOC included. The atomic contributions are color-coded. (f) The same spectra magnified in the vicinity of the Z point. Deep-pink and blue colors denote the bands localized in the BiTe_1 trilayer and the Bi-bilayer, respectively. A schematic view of the inversion of the bulk-band-gap edges for \mathbb{Z}_2 Topological Insulator (g) and Bi_2Te_1 (h). The bands with opposite parities are outlined by dashed and dotted lines; the violet ovals I–III indicate areas of the band inversion.

It was established that the majority of known strong \mathbb{Z}_2 TIs, like Bi_2Te_3 with the trigonal crystal structure, also accommodate a TCI phase and, thus, the Dirac state residing on the (111) surface is simultaneously protected by both the time-reversal and the crystal mirror symmetries. A magnetic field applied perpendicular to the mirror plane in Bi_2Te_3 destroys the \mathbb{Z}_2 topological phase and, hence, unravels the dual topological nature of the Γ Dirac state since the TCI phase is preserved and the Dirac surface state remains gapless¹⁵.

From this viewpoint, weak TIs are perspective for realization of a dual topological phase where the Dirac surface state of the \mathbb{Z}_2 topological phase and the topological states protected by the crystal symmetry can be manipulated separately without applying a magnetic field, owing to the fact that they appear at different crystal surfaces. In the following, we show that the weak 3D TI Bi_2Te_1 is a promising candidate.

This chemically stable crystalline compound is built by a periodic stack of two types of 2D fragments: BiTe_1 trilayers and Bi-bilayer¹⁶. Previously it was theoretically predicted that Bi_2Te_1 is a weak TI characterized by the (0; 0, 0, 1) \mathbb{Z}_2 invariant¹². Accordingly, calculations of the electronic structure of the (010) surface, which is not a natural cleavage surface of the compound, revealed TSS inside the bulk gap¹².

Herewith we present an *ab-initio* density-functional-theory study of the electronic structure of the Bi_2Te_1 natural cleavage (001) surface with different types of possible terminations. By means of these simulations we demonstrate for the first time that the $(\nu_1 \nu_2 \nu_3)$ surface of a weak 3D TI can accommodate a gapless spin-split surface state in the band gap. The preferable Te termination holds topological surface state, which opposite-spin branches cross at non-symmetric points of the 2D Brillouin zone (BZ) lying in the $\Gamma - \bar{M}$ directions ($\approx 0.3 |\Gamma - \bar{M}|$) where they are protected by mirror symmetry of the system of the system. Away from the $\Gamma - \bar{M}$ mirror plane a tiny gap of ≈ 8 meV opens up since the crossing is avoided by a symmetry constraint. On the contrary, the iodine- and $[\text{Bi}_2]$ -terminated surfaces of Bi_2Te_1 exhibit Rashba-like spin-split bands in the BZ center in addition to an even number of gapless $\Gamma - \bar{M}$ TSSs.

Results

The crystal structure of Bi_2Te_1 was elucidated from a single-crystal X-ray diffraction experiment¹⁶. The compound crystallizes in a centrosymmetric monoclinic unit cell (space group $C12/m1$, $a = 7.586$ Å, $b = 4.380$ Å, $c = 17.741$ Å, $\beta = 98.20^\circ$) with 16 atoms which can be represented as a Niggli-reduced cell ($a = b = 4.380$ Å, $c = 17.741$ Å, $\alpha = \beta = 82.9047^\circ$, $\gamma = 60.0025^\circ$) with 8 atoms [Fig. 1(a)]. We performed crystal growth experiments based on the synthetic protocol from¹⁶ and determined that the stacking sequence of layers and the lattice parameters are in agreement with the earlier reported results.

The layered Bi_2Te_1 structure comprises two 2D building blocks relevant for TI studies: the Bi-bilayer, $[\text{Bi}_2]$, which is theoretically predicted to be a 2D TI^{17,18}, and BiTe_1 trilayer, which is a structural unit of the BiTe_1 compound with giant Rashba-like spin splitting^{19–24}. The BiTe_1 compound can be tuned into a TI phase by external pressure²⁵. Moreover, a single BiTe_1 trilayer holds the giant Rashba state itself²⁶. These two types of fragments alternate in the stack in such a manner that the Bi-bilayers are always inserted between iodine atomic layers

forming [Te-Bi-I] · [Bi₂] · [I-Bi-Te] sandwiches. In contrast to covalent bonding within the [Bi₂] and the [I-Bi-Te] fragments, the sandwiches are held together by significantly weaker van-der-Waals interactions. As a result, the natural cleavage surface for Bi₂TeI is perpendicular to the (001) direction, and this ensures absence of trivial surface states within the bulk band gap. The material can be easily cleaved with scotch tape into thin flakes with three possible terminations: tellurium or iodine planes of the [Te-Bi-I] block, or bismuth bilayers. Our experimental results on cleavage show that the Te termination is predominant (more than 80% of instances). Furthermore, we estimated energies for the Te-Te and the Bi₂-I cleavages and found that the cleavage between adjacent [Te-Bi-I] · [Bi₂] · [I-Bi-Te] sandwiches, is ≈ 50 times more favorable than that between the [Bi₂] and the [I-Bi-Te] fragments, which is consistent with the experimentally found preference for the Te termination.

Stacked layers in the periodic Bi₂TeI structure are slightly shifted with respect to each other in the *ab* plane (this shift amounts to ca. 0.001 Å only within the unit cell). This forces the reduction of the trigonal point symmetry of the [Bi₂] and [I-Bi-Te] building blocks, respectively, down to the monoclinic symmetry of the entire Bi₂TeI crystal lattice. As a result, the BZ of the (001) surface is a slightly distorted hexagon with the base angles equal to 120.005 and 119.995 degrees, respectively. For this reason, the crystal structure can be regarded as a pseudo-hexagonal one in which only one mirror plane, $((-\bar{M}) - \bar{\Gamma} - \bar{M})$, is retained, whereas the other two mirror planes of the hexagonal lattice are transformed into pseudo-mirror planes $((-\bar{M}') - \bar{\Gamma} - \bar{M}'$ and $(-\bar{M}'') - \bar{\Gamma} - \bar{M}'')$, see Fig. 1(b). Below the influence of this small distortion from the trigonal symmetry on the electronic structure is discussed.

Spin-orbit interaction (SOC) plays a crucial role in this material. The electronic spectrum of Bi₂TeI without SOC included (Fig. 1(d)) has semimetallic character with a zero gap at the Z point. Switching on SOC transforms the electronic spectrum of Bi₂TeI from a semimetallic to an insulating one (Fig. 1(e)). Our calculation of the \mathbb{Z}_2 , determined from the product of the parity eigenvalues of the occupied states at the time-reversal invariant momenta (TRIM), confirms the (0; 0, 0, 1) indices obtained by Tang *et al.*¹². However, the SOC-induced band inversion is more complicated in this case than in conventional TIs, like Bi₂Te₃. In the latter, SOC lifts up the Kramers degeneracy in a valence-band-edge state (formed by Te *p*-orbitals) and a conduction-band-edge state (formed by Bi *p*-orbitals) at the TRIM. Since the strength of SOC is larger than the gap width, it leads to an inversion of the edge bands and formation of a new insulating gap owing to their hybridization (see a schematic picture in Fig. 1(g)). As can be seen from Fig. 1(d,e), the SOC-induced band inversion for the Bi₂TeI cannot be easily described in terms of atomic orbitals. Nevertheless, if one combines the orbitals that belong to different blocks (Fig. 1(f)) it can be deduced, firstly, that the bulk-band inversion in Bi₂TeI occurs between the states of the [Bi₂] and the [BiTeI] structural blocks, and, secondly, that two pairs of bands contribute to the SOC-induced band inversion in the resulting spectrum (shown schematically in Fig. 1(h)), in contrast to conventional TIs. The consequence of such complicated band inversion is that the band-gap-inversion area is not centered at the TRIM (see the indicated area I in Fig. 1(h)), as in the case of conventional TI. Furthermore, it triggers formation of additional hybridization gaps between the inverted bands in the valence and conduction bands (areas II and III, respectively). Based on these premises, emergence of a band-gap topological surface state at non-symmetric points as well as the valence- and conduction-band TSSs can be expected.

Simulations of the preferable Te-terminated surface were performed on a slab composed of four [Te-Bi-I] · [Bi₂] · [I-Bi-Te] sandwiches, i. e. of 32 atomic layers. Figure 2(a) shows the surface band-structure calculated without inclusion of SOC. This spectrum exhibits semimetallic character, so that the valence and conduction bands touch only at the $\bar{\Gamma}$ point and no surface states exist, as can be expected for a surface formed by cleavage through a van-der-Waals gap. The surface spectrum with included SOC (Fig. 2(b)) features a spin-polarized TSS that crosses the band gap along the $\bar{\Gamma} - \bar{K}$ and $\bar{\Gamma} - \bar{M}$ directions. Besides, additional spin-split TSSs arise in the valence and conduction bands. They are marked by violet circles II and III, respectively, in Fig. 2(b). Henceforward we focus solely on the band-gap TSS. This state is gapless with a crossing point (CP) lying at $\approx 0.3 \bar{\Gamma} - \bar{M}$ near the conduction band, whereas in the $\bar{\Gamma} - \bar{K}$ direction it has a tiny gap of 8 meV (Fig. 2(b)). Noteworthy is that the TSS comprises two degenerate states, one for each slab surface. For the considered slab thickness these states are slightly coupled, introducing an artificial minigap (of 2 meV) in the crossing point along the $\bar{\Gamma} - \bar{M}$ direction. The doubling of the slab in the *z* direction halves the size of this minigap, whereas the gap in TSS along the $\bar{\Gamma} - \bar{K}$ remains unchanged. Moreover, identical minigaps are also found in the $\bar{\Gamma} - \bar{M}'$ and $\bar{\Gamma} - \bar{M}''$ directions, thus leading to a conclusion that slight deviations from the trigonal structure in the title compound affect the energy spectrum even weaker than artifacts of the slab model. From these finding we can infer that the crystal-symmetry protection is tolerant (at least for the slab geometry) toward small structural distortions.

Energy dependence of the TSS in the full 2D BZ shows that the spin branches with opposite spins form two continuous surfaces with different spatial localization around the center of the BZ (see Fig. 2(c)). One surface (highlighted in yellow) is strongly localized in the outer [Te-Bi-I] trilayer, while the other one (in green) is localized in both [Te-Bi-I] and adjacent [Bi₂] blocks (see Fig. 2(d)). There is a tiny gap at the intersection of these two branches at all k_{\parallel} away of the $\bar{\Gamma} - \bar{M}$ mirror-planes, where the crossing is avoided by a symmetry constraint²⁷. The TSS remains gapless only in six CPs lying along the $\bar{\Gamma} - \bar{M}$ directions (marked by black dots in Fig. 2(c)), where it is protected by the crystal mirror symmetry.

The 2D Fermi Surface (FS) is composed of two Γ -centered contours (Fig. 2(e)) for various positions of the chemical potential within the entire bulk band gap. While the inner contour is almost circular, the outer one is subject to strong hexagonal warping. The inner branch of the TSS exhibits clockwise spin-rotation with a negligible out-of-plane spin component, whereas the outer, hexagonally warped branch demonstrates generally counter-clockwise helicity with a more complex spin-texture.

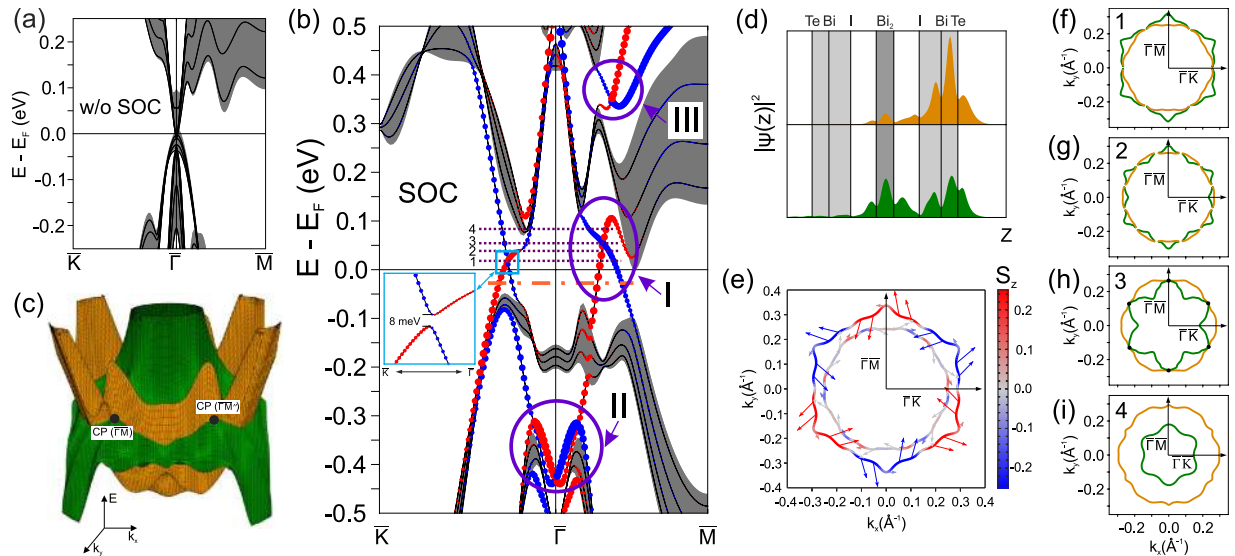


Figure 2. Electronic structure of the Te-terminated surface. The band structure of a Te-terminated Bi_2TeI (001) slab (black lines) and the projected bulk band structure (gray background) without (a) and with (b) spin-orbit coupling. The dots in the panel (b) represent weights of the states in the outer layers of the slab multiplied by a value of in-plane spin components S_x and S_y (red and blue colors denote the positive and negative projections of the spin vector \vec{S} on Cartesian axes, respectively). The violet ovals indicate: the gapless band-gap (I), the valence-band (II), and the conduction-band (III) TSSs. The inset shows a magnified view of the $\Gamma - \bar{K}$ tiny gap in the band-gap TSS. (c) A 3D view of the band-gap topological surface state. (d) Spatial distribution of the charge density integrated over (x, y) planes, $|\Psi(z)|^2$, for both branches of the band-gap TSS. Yellow and green colors accord with those in the panel (c). (e) Spin-resolved constant-energy contours (CECs) taken in the middle of the bulk gap (see the orange dash-dotted line in (b)). (f–i) CECs for the cuts 1–4 defined in the panel (b).

Let us consider the evolution of the 2D FS topology of the TSS at the energies above the conduction band minimum. Right above $E = 0$, where the TSS has a tiny gap in the $\Gamma - \bar{K}$ directions (see cut 1 in Fig. 2(b,f)), two Γ -centered contours transform into six pockets. At higher energies (cut 2 in Fig. 2(b,g)), the tiny TSS gap shifts away from the point on the high-symmetry direction which initiates further transformations in the FS from six to twelve pockets. Each pocket is centered at the points residing in high-symmetry directions. At $E = E_{CP}$ (cut 3 in Fig. 2(b,h)) the FS again evolves into two distinct Γ -centered contours so that the inner, camomile-like contour touches the outer one at the points lying along the $\Gamma - \bar{M}$ directions. Further shift of the chemical potential towards higher energies (cut 4 in Fig. 2(b,i)) leads to contraction(expansion) of the inner(outer) FS contour.

Let us now regard the less frequent iodine-terminated surface of Bi_2TeI . This case was approximated as an [I-Bi-Te] overlayer on top of the Te-terminated slab, so we consider mainly the changes that this add-on introduces in the electronic structure of the Te-terminated surface. The surface spectrum calculated without taking spin-orbit coupling into account (see Fig. 3(a)) is generally similar to the Te-terminated surface spectrum (see Fig. 2(a)) with an exception of a surface state residing at the Γ point at ≈ 0.2 eV in a local gap of the conduction band (marked by a deep pink curve). This state originates from the splitting of the upper edge of the first conduction band which is caused by positive band bending that is provided by the [I-Bi-Te] overlayer. This case bears similarity to the effects introduced by the iodine-terminated surface in the BiTeI compound²¹.

The switched-on SOC provokes significant modification of the surface electronic structure as compared to the case of the Te-terminated surface. First of all, SOC induces the bulk-band inversion, so that the bulk conduction band, from which the surface state is split off, dives into the valence band and, consequently, a trivial surface state emerges in the band gap (Fig. 3(b)). In spite of this modification the trivial surface state maintains its localization within the surface trilayers with a maximum in the outer trilayer (Fig. 3(c), deep pink and black curves in the outmost right panel) regardless of whether SOC is taken into account or not. Another consequence of the activated SOC is emergence of a Rashba-type spin splitting at small k_{\parallel} for the trivial surface state at $\bar{\Gamma}$. At larger k_{\parallel} the splitting acquires a more complicated character owing to hybridization of the trivial surface state with the topological one. This hybridization also substantially modifies the gapless spin-helical topological surface state which survives at $k_{\parallel} \approx 0.3 \bar{\Gamma} - \bar{M}$, although the energy of the CP noticeably lowers (with respect to its position at the Te-terminated surface) and approaches the bulk valence band (Fig. 3(b)). As far as localization of the TSS is concerned, the spatial distribution profiles for the opposite spin branches (Fig. 3(c), yellow and green curves) resemble those at the Te-terminated surface (Fig. 2(e)) with the difference that now they penetrate considerably into the [I-Bi-Te] overlayer.

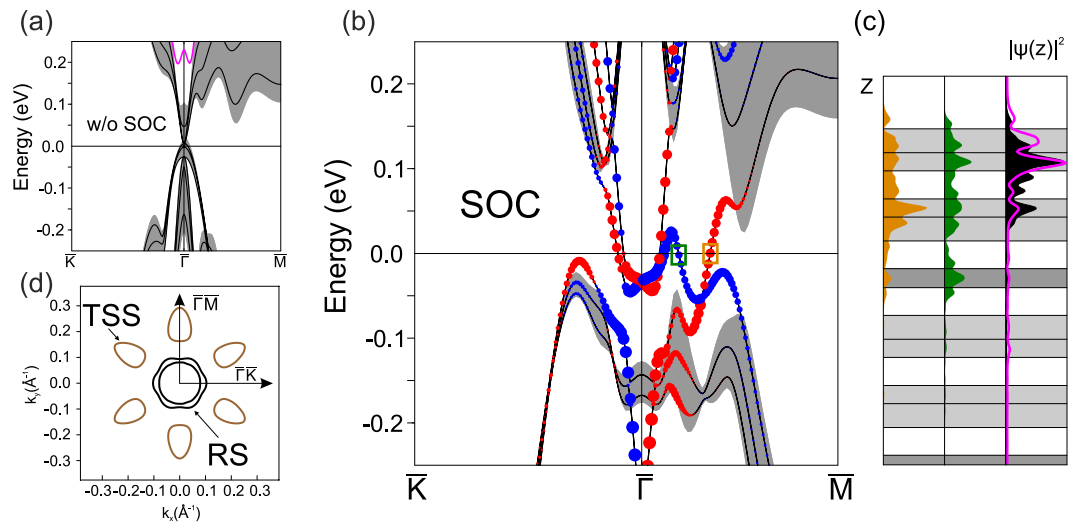


Figure 3. Electronic structure of the iodine-terminated surface. An energy spectrum of the iodine-terminated surface with spin-orbit coupling switched off (a) and on (b). (c) Spatial distribution of the charge density $|\Psi(z)|^2$ for the TSS branches corresponding to the positive (orange) and negative (green) spin projections (note the small colored squares in (b)) and for the trivial surface state at $\bar{\Gamma}$ with (black shading) and without (deep pink curve) including SOC. (d) Constant energy contours at the center of the bulk band gap.

Strong alternation of the electronic spectrum of the Bi_2TeI surface induced by the [I-Bi-Te] overlayer causes substantial changes in the 2D Fermi surface. In contrast to two $\bar{\Gamma}$ -centered contours provided by the topological surface state (Fig. 2(f)), it is now formed by six isolated egg-shaped pockets enclosing the TSS degeneracies plus two concentric contours from the Rashba-like trivial surface state (RS) in the vicinity of $\bar{\Gamma}$ (see Fig. 3(d)).

The last possible cleavage surface of Bi_2TeI is terminated by the Bi-bilayer and can be approximated as a $[\text{Bi}_2] \cdot [\text{I-Bi-Te}]$ overlayer on top of the Te-terminated surface or, alternatively, as a $[\text{Bi}_2]$ overlayer on top of the iodine-terminated surface.

First, the electronic structure of a freestanding $[\text{Bi}_2] \cdot [\text{I-Bi-Te}]$ overlayer is addressed. As can be seen from Fig. 4(a), its spectrum has a gap at the $\bar{\Gamma}$ point with a valence-band Rashba-split state at the Fermi level that is mostly localized in the $[\text{Bi}_2]$ -block in the vicinity of the $\bar{\Gamma}$ point, while away from this point the [I-Bi-Te] trilayer contributes predominantly to this state.

The Rashba-like state formed by the $[\text{Bi}_2] \cdot [\text{I-Bi-Te}]$ overlayer at the Fermi level is retrieved as the most prominent feature in the surface spectrum of the Bi_2 -terminated Bi_2TeI . Comparison of the spectra of a free-standing $[\text{Bi}_2] \cdot [\text{I-Bi-Te}]$ overlayer and the Bi_2 -terminated surface shows that the dispersion and spatial localization of the discussed state do not change (Fig. 4(d), left) as it remains localized in the $[\text{Bi}_2]$ block. The major difference is, however, that the spectrum is gapless in the case of the Bi_2 -terminated surface (see a light blue rectangle in Fig. 4(b)). This state with the CP at $\approx 0.25 \bar{\Gamma} - \bar{M}$ (Fig. 4(c)) below the conduction band can be regarded as the survived topological state which penetrated deeply into the adjacent sublayers down to a second trilayer (Fig. 4(d), right). The spin texture of this state is highly unusual because of the strong hybridization with the trivial Rashba state (Fig. 4(e)), namely, the spin, being mostly in-plane, always has a positive S_x component around the contour. The counterpart gapless state located in the $\bar{\Gamma} - (-\bar{M})$ direction has an opposite spin direction and, thus, the net spin equals zero over the Brillouin zone.

Methods

Crystal growth. A stoichiometric mixture of Bi, Te and BiI_3 (sublimated in vacuum prior to use) was placed into a silica ampoule that was then evacuated and sealed. The ampoule was heated to 823 K with a rate of 10 K/h, tempered for 2 hours and subsequently cooled down to ambient temperature with a rate 2 K/h. Largely overgrown crystalline platelets were found on the batch along with some single crystals that grew on the ampoule's walls. The products were characterized by semi-quantitative energy dispersive X-ray analysis (SU8020 (Hitachi) SEM, Silicon Drift Detector (SDD) $X - \text{Max}^N$ (Oxford)), X-ray diffractometry (X'Pert Pro MPD diffractometer (PANalytical), Ge(111) monochromator, Cu- K_α radiation) and TEM methods (FEI Titan F20 microscope with CS-correction operating at 80 kV). A typical SAED and HRTEM images for Bi_2TeI are given in Fig. 1(c) of the main text. The observed stacking sequence of layers and lattice parameters are in consistent with the those determined from the structure elucidation in ref. 16.

DFT calculations. Electronic structure calculations were carried out within the density functional theory using the projector augmented-wave method²⁸ as implemented in the VASP code^{29,30} and ABINIT code³¹. The PAW data sets in ABINIT code were taken from ref. 32. The exchange-correlation energy was treated using the generalized gradient approximation³³. The Hamiltonian contained the scalar relativistic corrections and the spin-orbit coupling was taken into account. The calculation of \mathbb{Z}_2 invariant was carried by using the parity of the

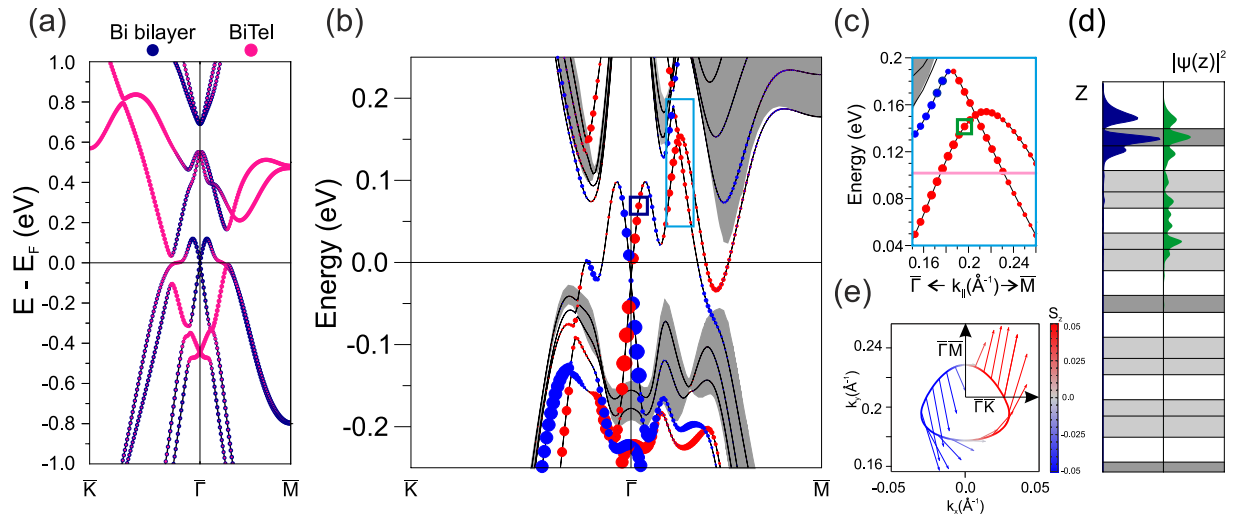


Figure 4. Electronic structure of a free-standing $[\text{Bi}_2] \cdot [\text{I-Bi-Te}]$ film and the Bi_2 -terminated surface. (a) Electronic spectrum of a $[\text{Bi}_2] \cdot [\text{I-Bi-Te}]$ film. (b) Band structure of the Bi_2 -terminated surface. (c) A magnified view of topological surface state in the $\Gamma - \bar{M}$ direction (note a light blue rectangle in the panel (b)). (d) Charge density distribution of the Rashba-like and topological surface states. The color scheme accords with the colors of the small squares in the panels (b,c). (e) Spin-resolved energy contour for $\Gamma - \bar{M}$ topological surface state below the CP (note a pink line in the panel (c)).

wave functions obtained in the framework of the Full Potential Linearized Augmented Plane wave (FLAPW) method implemented in FLEUR code³⁴. The bulk and surface spectra obtained using different codes are in full agreement.

References

- Hasan, M. Z. & Kane, C. L. *Colloquium: Topological insulators*. *Rev. Mod. Phys.* **82**, 3045–3067 (2010).
- Qi, X.-L. & Zhang, S.-C. Topological insulators and superconductors. *Rev. Mod. Phys.* **83**, 1057–1110 (2011).
- Vobornik, I. *et al.* Magnetic proximity effect as a pathway to spintronic applications of topological insulators. *Nano Lett.* **11**, 4079–4082 (2011).
- Fu, L. & Kane, C. L. Topological insulators with inversion symmetry. *Phys. Rev. B* **76**, 045302 (2007).
- Liu, C.-X., Qi, X.-L. & Zhang, S.-C. Half quantum spin Hall effect on the surface of weak topological insulators. *Physica E: Low-dimensional Systems and Nanostructures* **44**, 906–911 (2012).
- Yan, B., Müchler, L. & Felser, C. Prediction of weak topological insulators in layered semiconductors. *Phys. Rev. Lett.* **109**, 116406 (2012).
- Hou, J.-M., Zhang, W.-X. & Wang, G.-X. Three-dimensional topological insulators in the octahedron-decorated cubic lattice. *Phys. Rev. B* **84**, 075105 (2011).
- Yang, G., Liu, J., Fu, L., Duan, W. & Liu, C. Weak topological insulators in PbTe/SnTe superlattices. *Phys. Rev. B* **89**, 085312 (2014).
- Rasche, B. *et al.* Stacked topological insulator built from bismuth-based graphene sheet analogues. *Nat. Mater.* **12**, 422–425 (2013).
- Rasche, B. *et al.* Crystal growth and real structure effects of the first weak 3d stacked topological insulator $\text{Bi}_{14}\text{Rh}_3\text{I}_9$. *Chem. Mater.* **25**, 2359–2364 (2013).
- Pauly, C. *et al.* Subnanometre-wide electron channels protected by topology. *Nat. Phys.* **11**, 338–343 Letter (2015).
- Tang, P. *et al.* Weak topological insulators induced by the interlayer coupling: A first-principles study of stacked Bi_2TeI . *Phys. Rev. B* **89**, 041409 (2014).
- Fu, L. Topological crystalline insulators. *Phys. Rev. Lett.* **106**, 106802 (2011).
- Ando, Y. & Fu, L. Topological crystalline insulators and topological superconductors: From concepts to materials. *Annu. Rev. Condens. Matter Phys.* **6**, 361–381 (2015).
- Rauch, T., Flieger, M., Henk, J., Mertig, I. & Ernst, A. Dual topological character of chalcogenides: Theory for Bi_2Te_3 . *Phys. Rev. Lett.* **112**, 016802 (2014).
- Savilov, S. V., Khrustalev, V. N., Kuznetsov, A. N., Popovkin, B. A. & Antipin, M. Y. New subvalent bismuth telluroiodides incorporating Bi_2 layers: the crystal and electronic structure of Bi_2TeI . *Russ. Chem. Bull., Int. Ed.* **54**, 87–92 (2005).
- Murakami, S. Quantum spin Hall effect and enhanced magnetic response by spin-orbit coupling. *Phys. Rev. Lett.* **97**, 236805 (2006).
- Wada, M., Murakami, S., Freimuth, F. & Bihlmayer, G. Localized edge states in two-dimensional topological insulators: Ultrathin Bi films. *Phys. Rev. B* **83**, 121310 (2011).
- Ishizaka, K. *et al.* Giant Rashba-type spin splitting in bulk BiTeI . *Nat. Mater.* **10**, 521–526 (2011).
- Sakano, M. *et al.* Strongly spin-orbit coupled two-dimensional electron gas emerging near the surface of polar semiconductors. *Phys. Rev. Lett.* **110**, 107204 (2013).
- Eremeev, S. V., Nechaev, I. A., Koroteev, Y. M., Echenique, P. M. & Chulkov, E. V. Ideal two-dimensional electron systems with a giant Rashba-type spin splitting in real materials: surfaces of bismuth tellurohalides. *Phys. Rev. Lett.* **108**, 246802 (2012).
- Eremeev, S. V., Nechaev, I. A. & Chulkov, E. V. Giant Rashba-type spin splitting at polar surfaces of BiTeI . *JETP Lett.* **96**, 437–444 (2012).
- Crepaldi, A. *et al.* Giant ambipolar Rashba effect in the semiconductor BiTeI . *Phys. Rev. Lett.* **109**, 096803 (2012).
- Landolt, G. *et al.* Disentanglement of surface and bulk Rashba spin splittings in noncentrosymmetric BiTeI . *Phys. Rev. Lett.* **109**, 116403 (2012).
- Bahramy, M., Yang, B.-J., Arita, R. & Nagaosa, N. Emergence of non-centrosymmetric topological insulating phase in BiTeI under pressure. *Nat. Commun.* **3**, 679 (2012).
- Eremeev, S. V., Tsirkin, S. S., Nechaev, I. A., Echenique, P. M. & Chulkov, E. V. New generation of two-dimensional spintronic systems realized by coupling of Rashba and Dirac fermions. *Sci. Rep.* **5**, 12819 (2015).

27. Weber, A. P. *et al.* Gapped surface states in a strong-topological-insulator material. *Phys. Rev. Lett.* **114**, 256401 (2015).
28. Blöchl, P. E. Projector augmented-wave method. *Phys. Rev. B* **50**, 17953–17979 (1994).
29. Kresse, G. & Furthmüller, J. Efficient iterative schemes for ab initio total-energy calculations using a plane-wave basis set. *Phys. Rev. B* **54**, 11169–11186 (1996).
30. Kresse, G. & Joubert, D. From ultrasoft pseudopotentials to the projector augmented-wave method. *Phys. Rev. B* **59**, 1758–1775 (1999).
31. Gonze, X. *et al.* Abinit: First-principles approach to material and nanosystem properties. *Computer Physics Communications* **180**, 2582–2615 (2009).
32. Jollet, F., Torrent, M. & Holzwarth, N. Generation of projector augmented-wave atomic data: a 71 element validated table in the xml format. *Comp. Physics Comm.* **185**, 1246–1254 (2014).
33. Perdew, J. P., Burke, K. & Ernzerhof, M. Generalized gradient approximation made simple. *Phys. Rev. Lett.* **77**, 3865–3868 (1996).
34. URL: <http://www.flapw.de>.

Acknowledgements

This work is supported by grant (No 8.1.05.2015) from the Tomsk State University Academic D.I. Mendeleev Fund Program and the St. Petersburg State University (project no. 11.50.202.2015). Calculations were performed on the SKIF-Cyberia supercomputer of Tomsk State University. A. I. acknowledges the Priority Program 1666 “Topological Insulators” of the Deutsche Forschungsgemeinschaft (DFG, grant No. IS 250/1-1) and is grateful to M. Richter and K. Koepnik (IFW Dresden) for fruitful discussions, to U. Kaiser and C. T. Koch (Ulm University) for providing beam time for the TEM characterization, to E. Schmid (Ulm University) for ultramicrotomy.

Author Contributions

The calculations were performed mainly by I.P.R., T.V.M. and S.V.E. with contributions by Y.M.K. and M.G.V. Experiments were performed by A.I. The idea of the study was proposed by E.V.C., who is the supervisor of the project, A.I. and P.M.E. All authors contributed to discussion, data analysis. I.P.R., T.V.M., S.V.E., A.I. and E.V.C. wrote the manuscript.

Additional Information

Competing financial interests: The authors declare no competing financial interests.

How to cite this article: Rusinov, I. P. *et al.* Mirror-symmetry protected non-TRIM surface state in the weak topological insulator Bi₂TeI. *Sci. Rep.* **6**, 20734; doi: 10.1038/srep20734 (2016).



This work is licensed under a Creative Commons Attribution 4.0 International License. The images or other third party material in this article are included in the article's Creative Commons license, unless indicated otherwise in the credit line; if the material is not included under the Creative Commons license, users will need to obtain permission from the license holder to reproduce the material. To view a copy of this license, visit <http://creativecommons.org/licenses/by/4.0/>